Contrib. Astron. Obs. Skalnaté Pleso **40**, 107 – 129, (2010)

The populations of the trans-Neptunian small bodies from the simulation of the Oort-cloud formation

M. Jakubík[1], G. Leto[2] and L. Neslušan[1]

[1] *Astronomical Institute of the Slovak Academy of Sciences*
059 60 Tatranská Lomnica, The Slovak Republic,
(E-mail: mjakubik@ta3.sk, ne@ta3.sk)

[2] *Catania Astrophysical Observatory*
Via Santa Sofia 78, I-95123 Catania, Italy, (E-mail: giuseppe.leto@oact.inaf.it)

Received: July 7, 2010; Accepted: October 12, 2010

Abstract. Considering the model of the initial disc of planetesimals consisting of 14 799 test particles, we simulated the formation of the populations of small bodies in the outer region of the solar system for an initial 2 -Gyr period. We aimed to provide a common reference model of the formation of all inner and outer parts of the Oort cloud. In this paper, we deal with a picture of the trans-Neptunian-belt populations which can be outlined within our simple model. The dynamical evolution of massless test particles is followed via numerical integration of their orbits. We consider perturbations by four giant planets in their current orbits and with their current masses, as well as perturbations by the Galactic tide and passing stars. Our simulation qualitatively reproduces almost all structural features observed in the trans-Neptunian region. Unfortunately, there are a lot of quantitative discrepancies between our model and observed reality implying the main conclusion that the assumption of a dynamically very cold initial proto-planetary disc (with eccentricity $\sim$0.01 and inclination $\sim$0.01 rad), which extends beyond the heliocentric distance of about 34 AU, is inconsistent with the observed structure of trans-Neptunian population of small bodies. A big discrepancy is the survival of an almost untouched initial model population beyond $\sim$34 AU which is not observed. Two following positive observed details of the TN-population structure can, perhaps, be explained with the help of our simple model. Concerning the first, we showed that the outer border of the range of Neptune's perturbation on the dynamically cold orbits is identical with the outer border of 2:1 mean-motion resonance with this planet, where a sharp decrease of the number density of bodies belonging to the classical Edgeworth-Kuiper belt is observed. Most probably, this decrease is related to Neptune's ability to significantly influence the motion of small bodies, if we assume that these bodies formed closer to the Sun and were transported into the belt by Neptune. Second, the outer border of the objects of the so-called detached subpopulation is approximately at the same heliocentric distance of 100 AU in both model and observational samples.

Key words: Kuiper Belt – Solar system: formation

1. Introduction

The databases of the known populations of small bodies at the outer region of the solar system have been permanently increasing. This circumstance enables refinement of our knowledge about the formation, evolution, and structure of these populations. In the near future, an effort to create a unified theory, including all populations, can be expected. It should replace the former partial theories providing a description of each population separately, but not always in consistency with each other. Moreover, the new theory should also include the last stage of the formation of Jovian planets.

In our previous works (Dybczyński et al., 2008; Leto et al., 2008; these works are referred to as Paper I and Paper II, hereinafter), we performed a simulation of the evolution of a primordial proto-planetary disc (PPD, hereinafter) considering test particles (TPs) as massless. We used the GRID-computing technique that is sufficient if real planetesimals or cometary nuclei are approximated with massless particles. In more detail, we considered the model of the initial disc of planetesimals, which was represented by 10 038 TPs, and studied their dynamics during 2 Gyr, when influenced by perturbations of the four giant planets (in their current orbits and with their current masses), the galactic tide, and nearby passing stars. A more detailed description of the initial conditions and the computational procedure used can be found in Paper I. Based on this simulation, we described the formation and some structural characteristics of the outer (Paper I) and inner (Paper II) Oort cloud (OC).

In the present work, we use the resultant data from the former simulation and describe the formation process, further dynamical evolution, and some features of the structure of small-body trans-Neptunian (TN) populations.

It is necessary to mention some older models concerning the dynamical evolution of the TN populations. In an attempt to explain the relatively eccentric and high-inclined orbit of Pluto, Malhotra (1993) assumed a migration of Jovian planets. The migration can be explained by an interaction of a giant planet with planetesimals in the outer part of the planetesimal disc. The TN populations were mostly influenced by a smooth outward migration of Neptune.

Another model assuming the migration of Jovian planets was the so-called Nice model (Tsiganis et al., 2005). According its first version, the simulation of planetary-system dynamics started in a more compact configuration, with Jupiter, Saturn, Neptune, and Uranus at the heliocentric distances of 5.45, $\sim$8.2, $\sim$11.5, and $\sim$14.2 AU, respectively. Beyond the orbit of Uranus, a massive planetesimal disc was suggested to exist. It spanned from $\sim$15 to $\sim$34 AU and had the total mass of $\sim$35 Earth masses. On a time scale of hundred million years to billion years, Jupiter and Saturn crossed their mutual 2:1 mean motion resonance (MMR). The system went unstable, the aphelia of Neptune and Uranus were enlarged, therefore these planets crossed the outer planetesimal disc shaping its structure. Immediately after the period of instability started, Neptune and Uranus interchanged their mutual position with respect to the Sun. During the period of instability, Jupiter migrated slightly inward, while Saturn, Uranus, and Neptune migrated outward up to their currently observed heliocentric distances. This migration trend was already found by Malhotra (1993). According the later version of the Nice model, Jupiter and Saturn started near their 3:2 MMR (Morbidelli & Crida, 2007). However, the main evolutionary features of the system are the same.

The models comprising the planet migration have been successful to explain several features observed in the TN region. In particular, it is a low observed total mass of the TN population. This mass is two to three orders of magnitude lower than expected if the TN objects accreted in situ. The migration models require the outer edge of the planetesimal disc at a distance not much greater than the current orbit of Neptune. Otherwise, the outward migration of this planet would have to continue. The current TN populations were formed by Neptune, which trapped the bodies in the MMRs. As Neptune's orbit was enlarged, the orbits of objects in these MMRs were enlarged. This mechanism explains, at the same time, several times larger number of objects in 3:2 MMR than 2:1 MMR. (In our model without the planet migration, we shall see that the opposite ratio is predicted.)

Our simple model of the OC formation ignores the drag force of the solar-nebula remnant gas (e.g. Brasser et al., 2007) and, especially, the gradual growth and migration of giant planets, which is an essential feature of recent models (e.g. Tsiganis et al., 2005). Nevertheless, we believe that there are still some reasons to map which observed TN structures and mechanisms leading to their occurrence can be reproduced already within the simple model considered. The comparisons of similar simple models with the observed reality were done, as far as we know, in the era of the discovery of the few first TN objects (e.g. Holman & Wisdom, 1993; Levison & Duncan, 1993). A new comparison of the model, which is simple but encompasses the whole TN population, with a meanwhile much larger database of known TN objects can be useful. If nothing else, the comparison summarizes a lot of the discrepancies that are necessary to be explained within more sophisticated models.

2. Some remarks on various issues

In Paper I, we found, surprisingly, that a significant fraction of cometary nuclei came to the outer OC from the region $\sim 40-42$ AU, whereby we considered the PPD up to 50 AU. In the light of this fact, we regard as useful to map also the dynamical evolution in a region beyond the observed outer edge of the classical Edgeworth-Kuiper belt (CEKB) at 50 AU to check if this part of the PPD, if actually populated, could be dynamically active. So, we perform an additional simulation of the evolution of the outer part of the PPD situated at heliocentric distances from 50 to 90 AU. In the additional simulation, this part of the PPD is represented by another 4761 TPs. Their initial orbits are modelled to be consistent with the more inner part of the PPD. The profile of the PPD surface-density distribution proportional to $r^{-3/2}$ (r is the heliocentric distance) is preserved and other initial characteristics remain also the same as in the first simulation (see a detailed description in Sect. 2.1 of Paper I). In total, we use the resultant data, for 2 Gyr, of 14 799 TPs representing part of the initial PPD from 4 to 90 AU.

Dealing with individual groups of small bodies, it is necessary to specify criteria to classify a given body into a particular group. In other words, one must accept a nomenclature of the studied bodies. However, the populations of the TN bodies have been discovered relatively recently, therefore their structure is still under study and definition still evolving. Since a unique classification is necessary despite the evolving situation, we adopt the nomenclature of the outer solar system recently proposed by Gladman et al. (2008). A single change is made: to investigate the evolution of a resonance parameter (elongation angle) for distinguishing a MMR, we do not follow the future evolution for 10 Myr, but only for 1 Myr. As well, we follow the evolution of only the best-fit orbit (Gladman et al. suggested to follow also the evolution of orbits that are extremes of the orbital uncertainty in semi-major axis). In this work, we convert our simulation data, originally referred to in the modified galactic coordinate system, to the ecliptical coordinate system which is suitable for the study of objects more or less associated with the ecliptic.

To compare, at least roughly, our results from the simulation with the observational data, we select the corresponding actually discovered objects from the database of asteroids, Centaurs, and TN objects downloaded from the Minor Planet Center web site (`http://www.cfa.harvard.edu/iau/MPCORB.html`) on July 3, 2009. At that time the database contained the orbits of 399 919 objects. Of course, we are only interested in the objects with the semi-major axis corresponding to the studied TN region ($a > 28$ AU). Moreover, the newly-determined orbits are not expected to be very precise. For comparison, we therefore use a sample of only those large-a objects, which were observed at three or more oppositions. In total, 675 objects of the TN population meet our criteria.

A direct comparison between theoretical and observational data is impossible due to observational selection effects. For a simulated distribution of a given position parameter, we imitate the primary selection effects that occur due to the decrease of apparent brightness of objects with increasing heliocentric and geocentric distances. We neglect effects due to the inhomogeneity of observations searching for those TN objects in the sky that were concentrated mainly near the ecliptic. These effects are practically impossible to be described and, so, imitated. Although the imitation of the primary selection effects is not completely sufficient, it still helps us to reveal a trend of the bias in a given distribution that can be expected due to an observational selection.

In particular, we imitate an observational bias associating a certain weight, w, to each TP. A given TP in our considerations represents an aggregate of

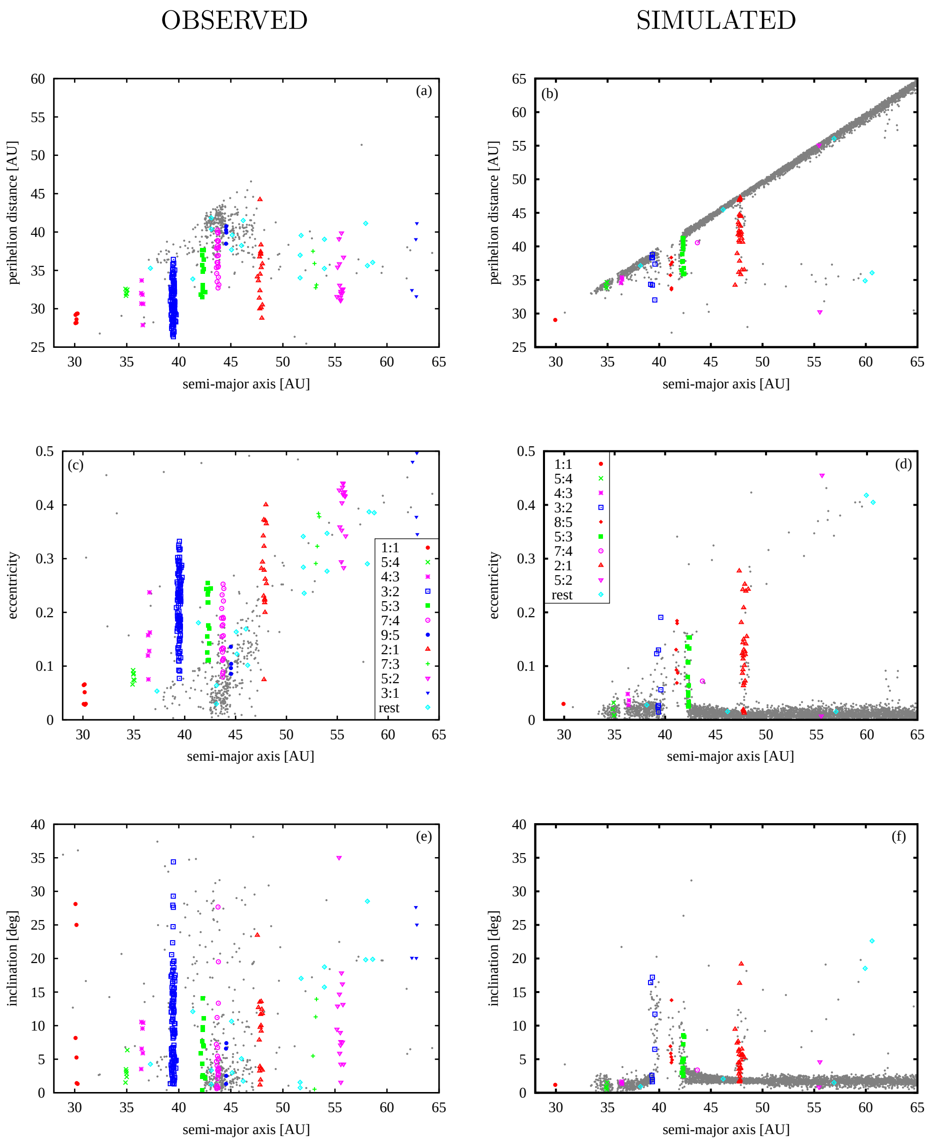

Figure 1. The distribution of the observed and simulated objects, which are in the MMRs with Neptune in the $q-a$ (plots a,b), $e-a$ (c,d), and $i-a$ (e,f) phase spaces. The left plots (a, c, and e) show the observed distributions and right plots (b, d, and f) show their modelled counterparts at 2 Gyr. The objects in MMRs are shown by various symbols, black-and-white in the printed and colour in the electronic version of the figure. The small gray full circles show the positions of all non-resonant objects.

bodies of all possible sizes, corresponding to a variety of absolute brightness, which are assumed to be uniformly distributed along the orbit of a TP. The weight is proportional to the number of all visible objects in a given orbit. In the calculation of the contribution to the weight for a given size-interval of bodies at a given distance, Δw, it is also necessary to take into account a time factor. An object spends time τ in a distance interval from $r - \Delta r$ to $r + \Delta r$. This time is longer for a more slowly moving object, therefore its discovery probability in this distance interval is greater than that of a faster object of the same absolute brightness. So, Δw is also proportional to τ.

According Trujillo et al. (2001), a size distribution of the radii of objects in the CEKB, R, can be approximated by a power law

$$n(R)\,dR = K_R R^{-s}\,dR, \tag{1}$$

with $s \doteq 4.0$. Assuming that this distribution can be generalized to the whole TN population and taking into account the fact that there are two known objects, Eris and Pluto, with the radius of about 1 000 km, we can gauge the distribution (constant K_R) as

$$K_R = 2(s-1)R_{up}^{s-1}, \tag{2}$$

where $R_{up} = 1\,000$ km.

Of course, an object is observable and can be detected only if it reaches or exceeds a certain threshold limit of apparent brightness. Since the typical surface colour of TN objects is red, these objects are usually discovered and observed in the red filter of the UBVRI system. Taking this into account, the magnitudes that we deal with below are red magnitudes. If we denote the object's apparent magnitude by m and the limiting magnitude by m_{lim}, it must be valid that $m < m_{lim}$. The apparent brightness can be calculated by the well-known formula (e.g. Trujillo et al., 2001)

$$m = m_{\odot} - 2.5\,log_{10}[A_R\Phi(\alpha')R^2] + 5\,log_{10}(1.496 \times 10^8 r r_g), \tag{3}$$

where $m_{\odot} = -27.1$ is the apparent red magnitude of the Sun, A_R is the geometric red albedo (we adopt $A_R = 0.04$, i.e. the value consistent with a dark Centaur-like albedo), $\Phi(\alpha')$ is Bowell et al.'s (1989) phase function, and r_g is the geocentric distance of a TP. Assuming that objects are observed near their opposition, we put $r_g \doteq r - 1$ AU and $\alpha' = 0$. The latter implies $\Phi(0) \doteq 1$.

To obtain the first contribution Δw of the weight of a given TP, we calculate the apparent magnitude, m, for the object of the largest radius R_{up} at distance r. The weight contribution is zero if $m > m_{lim}$. Otherwise, we set the initial value $\Delta w = 2$ (accounting for Eris- and Pluto-sized objects). Then, we integrate the distribution (1) from $R_{up} - \Delta R$ to R_{up} and calculate the apparent magnitude for $R = R_{up} - \Delta R/2$ by (3). If $m \leq m_{lim}$, the result of integration is added to w. The integration goes on for a decreasing upper R (about ΔR, whereby we arbitrarily choose $\Delta R = 1$ km) and we keep adding the results to w until m becomes larger than m_{lim}. This procedure is made for every heliocentric distance interval ranging from the perihelion to aphelion of the considered TP-orbit.

3. The resonant trans-Neptunian population

In the old literature, the Edgeworth-Kuiper belt (EKB) was mentioned to consist of the CEKB and a resonant component, i.e. objects being in the MMRs with Neptune. However, some MMRs appear to be rather related to a scattered disc (SD) than to the EKB, therefore we regard the whole resonant population as an extra group.

The structure of the resonant population, as implied by our simulation, and a comparison between our theoretical model and actually observed structure are discussed in this section. We are interested in the outer MMRs and 1:1 MMR with Neptune. So, we deal only with bodies in orbits having the semi-major axis $a \gtrsim 28\,\mathrm{AU}$.

According to Gladman et al. (2008), an object is in the k:k_N MMR with Neptune, if its semi-major axis corresponds to the orbital period being the k/k_N-multiple of Neptune's orbital period and the resonant argument

$$\sigma = k_N \lambda_N - k\lambda - (k_N - k)\tilde{\omega} \tag{4}$$

oscillates around a certain value (most often around 180^o), i.e. the interval of all its values occurring during the whole evolution-follow-up period (of 1 Myr according to our own choice) is smaller than 360^o. k and k_N are natural numbers, λ and λ_N are mean longitudes of the object and Neptune, respectively, and $\tilde{\omega}$ is the longitude of perihelion of the object. In our search for the MMRs, we also consider relatively high values of k and k_N; in particular, k ranges from 1 to 50 and k_N from 1 to $k-1$.

A list of known well-populated MMRs is given in Table 1. In more detail, only the MMRs consisting of four or more objects in at least one group (observed or modelled) are listed in this table. The modelled MMRs are classified at the end of the simulation, at 2 Gyr. In the observational data, we found, in addition, another 19 MMRs. One of them (9:4) consists of 3 objects, four of 2 objects (8:3, 11:6, 12:5, and 12:7), and fourteen of only a single object (4:1, 5:1, 7:2, 8:5, 10:3, 11:2, 11:8, 17:9, 18:1, 19:7, 19:10, 20:1, 22:5, and 36:1). In the simulation, when no observational bias is considered, 12 MMRs occur in addition to those in Table 1. Specifically, the MMR 8:3 consists of 2 TPs and the other 11 MMRs (5:1, 7:2, 10:1, 10:7, 13:5, 14:3, 14:5, 16:3, 19:10, 20:7, and 31:3) of a single TP.

The relative abundances of the MMRs are shown in Fig. 2. The abundances of the modelled MMRs can be seen in plot (a). The predicted observable abundances after the imitation of the basic observational bias, assuming the power-law size distribution of the resonant TNOs with $s = 4.0$ (Trujillo et al., 2001), are shown in plot (b). The bias reduces the discrepancy in the relative ratio of 3:2 and 2:1 MMRs. However, the MMRs 1:1, 5:4, 4:3, 8:5, and 5:3 become clearly overabundant in the model, when compared with the relative ratios of the observed MMRs (Fig. 2c). The models of the TN-region dynamical evolution considering the planet migration (see Sect. 1) can much better explain the higher abundance of objects in MMR 3:2 in comparison to that in MMR 2:1.

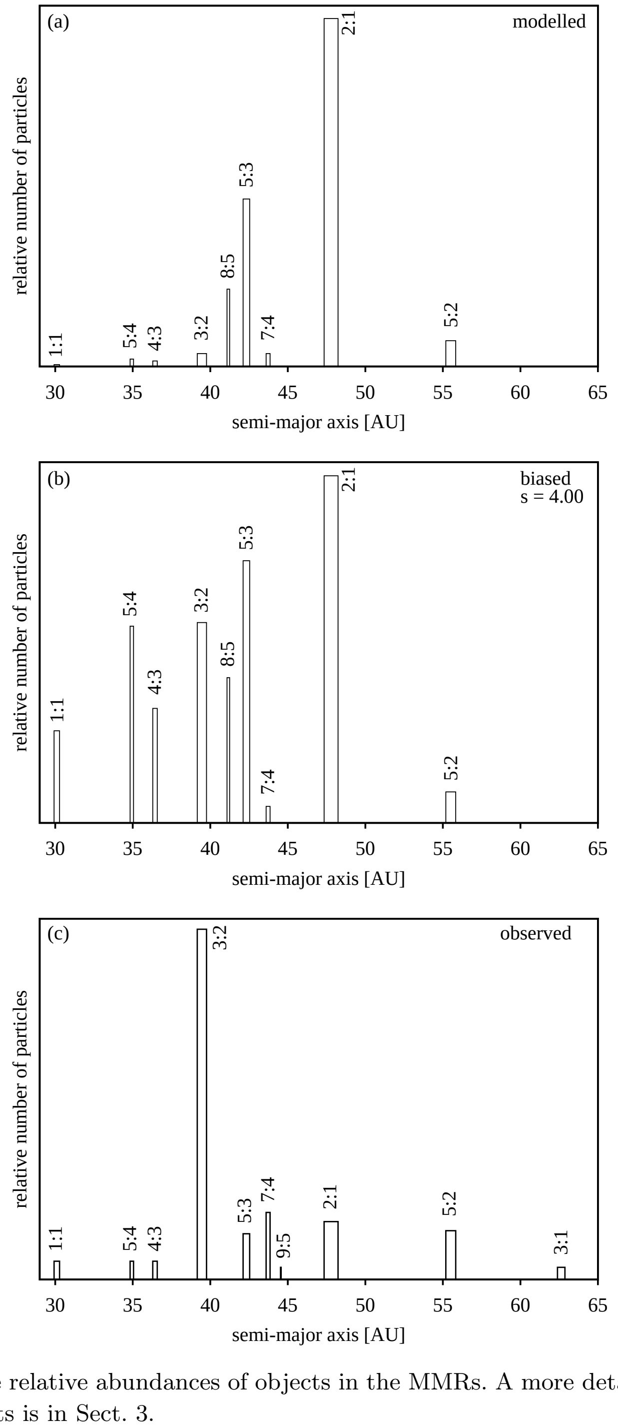

Figure 2. The relative abundances of objects in the MMRs. A more detailed description of the plots is in Sect. 3.

Table 1. The outer MMRs with Neptune containing 4 and more either observed or theoretical objects. The absolute theoretical numbers do not correspond with the observed numbers, therefore only relative abundances in both sets can be compared. N is the number of objects found in a given MMR and N_b is the number of TPs in a given MMR in the simulation when the observational bias is imitated. The value of the index of a power-law size distribution of TNOs is considered to be equal to $s = 4.0$.

	observed		modelled		
MMR	N	a-range [AU]	N	N_b	a-range [AU]
1:1	6	30.1−30.3	1	3.217	
5:4	6	34.9−35.0	4	6.873	34.8−34.9
4:3	6	36.4−36.6	3	3.999	
3:2	107	39.2−39.8	7	7.000	39.2−39.6
8:5	1		6	5.077	41.1−41.2
5:3	14	42.1−42.5	13	9.160	42.2−42.4
7:4	22	43.6−43.9	1	0.577	
9:5	4	44.5−44.6	0	−	
2:1	17	47.5−48.0	27	12.126	47.3−48.2
7:3	4	52.9−53.2	0	−	
5:2	15	55.2−55.8	2	1.085	
3:1	4	62.4−62.9	0	−	

The trapping of objects in the closer-to-Neptune 3:2 MMR is stronger than the traping in the more distant 2:1 MMR, therefore a smaller number of objects can escape from the 3:2 MMR during Neptune's migration.

To achieve a better agreement of the model with the observed MMR abundances, we can also consider (i) size distributions with indices higher, in principle, than 4.0, and (ii) steeper profiles of the surface density of the initial PPD. Concerning the initial-PPD surface-density profile, Kusaka et al. (1970; see also Weidenschilling, 1977) found an acceptable heliocentric-distance variability of this parameter from about $\propto r^{-2}$ to $\propto r^{-1}$. We can modify our original $\propto r^{-3/2}$ surface-density profile assigning the appropriate weights to the TPs according to their initial heliocentric distance. A reduction of the abundances of the MMRs inside the Plutinos appears, however, too small to predict the observable number even for the steepest acceptable profile of $\propto r^{-2}$. In addition, the discrepancy between the relative Plutinos and 2:1 MMRs increases for this profile.

The same problem occurs when we imitate the observational bias assuming a higher index of the slope of the size distribution. The increase of this parameter above the value of 4.0 is also problematic because lower values are rather expected. Levison & Stern (2001) determined $s = 3.0$ for large TNOs of the hot subpopulation. Davis & Farinella (1997) argued that collisions were important in the early evolution of the EKB. If a collisional steady-state was reached, then the value of s-index should be $5/3 < s < 2$ (Dohnanyi, 1968). Although the assumption of a full steady-state is not sure, the importance of collisions likely indicates a lower than a higher value of s than 4.0.

A qualitative inspection of occurrence or absence of objects in the observed and modelled resonant populations reveals qualitative agreement of our model with the observed reality. The most abundant observed MMRs (3:2, 7:4, 2:1, 5:2, and 5:3) are reproduced in the simulation. Except for the 9:5, 7:3, and 3:1 MMRs, other well-populated observed MMRs have at least a single TP in the simulated counterpart.

To complete the list of differences, we note that MMR 8:5 appears to be quite numerous in the model, but it is absent in the observational data. An intriguing MMR appears to be the observed 3:1 MMR. Starting with our dynamically very cold initial population, this MMR is not reproduced after 2 Gyr.

The MMRs with Neptune are also shown in the $q-a$ (plots a,b), $e-a$ (c,d), and $i-a$ (e,f) phase spaces in Fig. 1. The left plots (a, c, and e) show the observed distributions and right plots (b, d, and f) show their modelled counterparts at 2 Gyr. A specific symbol is used to show the position of an object that is in the MMR consisting of more than three objects. The less-than-four-object MMRs are also shown in the displayed interval of a, but all with the blue diamond. The gray full circles show the positions of all non-resonant objects.

4. The scattering-disc and detached objects

There are three groups of the non-resonant TN objects: scattering disc objects (SDOs), detached trans-Neptunian objects (DTNOs), and CEKB objects. According to Gladman et al. (2008), the SDOs and DTNOs are characterized by semi-major axis, a, satisfying $a_N < a < a_{in}$ (a_N is the Neptune's semi-major axis and a_{in} is the inner border, in terms of semi-major axis, of the OC), except for objects with both the Tisserand parameter with respect to Jupiter $T_J < 3.05$ and perihelion distance $q < 7.35$ AU. Following the dynamical evolution of the non-resonant objects for 1-Myr period, the SDOs are characterized by the magnitude of change of the semi-major axis $|\Delta a| > 1$ AU, while the DTNOs have $|\Delta a| \leq 1$ AU. (Gladman et al. used the limit $|\Delta a| = 1.5$ AU, but regarded the whole interval from 1 to 2 AU as acceptable. Since we reduced the period during which we follow the dynamical evolution, we use the lower limit of the interval in our considerations.) The eccentricity of DTNOs must, in addition, satisfy $e > 0.24$.

The SDO and DTNO populations are shown in Fig. 3 in $q-a$ (plots a and b), $e-a$ (c and d), and $i-a$ (e and f) spaces. The left plots (a, c, and e) show the observed SDOs and DTNOs, while the right plots (b, d, and f) show these groups in the model. A comparison between plots a and b showing the $q-a$ distributions reveals a lot of observed SDOs as well as DTNOs with a relatively small perihelion distance. The perihelia of DTNOs can reach the vicinity of Uranus' orbit and those of SDOs the vicinity of Saturn's orbit. On the contrary,

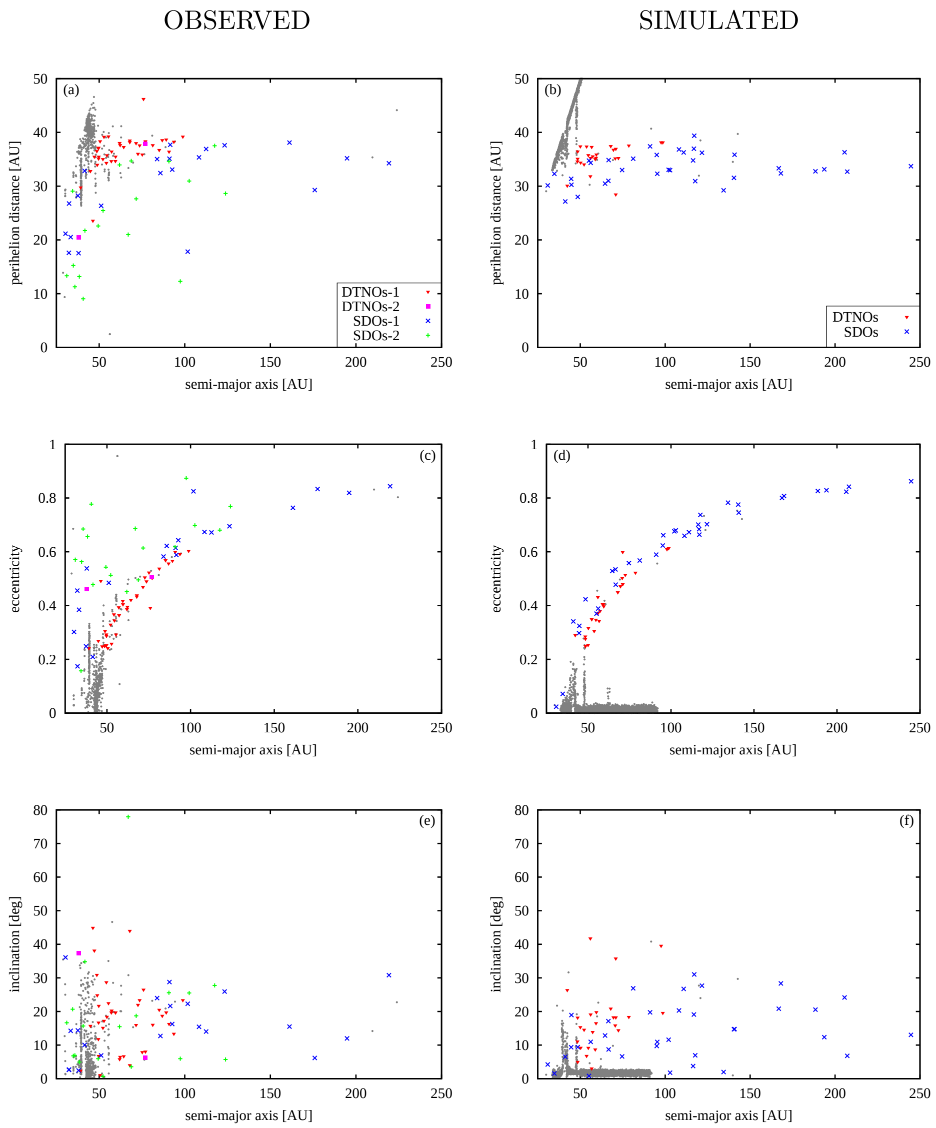

Figure 3. The distribution of the simulated TPs and observed objects, which are classified as the SDOs and DTNOs, in the $q-a$ (plots a, b), $e-a$ (c, d), and $i-a$ (e, f) phase spaces. The left plots (a, c, and e) show the observed distributions and right plots (b, d, and f) show their simulated counterparts at 2 Gyr. The SDOs and DTNOs are shown by various symbols, black-and-white in the printed and colour in the electronic version of the figure. The small gray full circles show the positions of all objects belonging to the other groups. The DTNOs and SDOs labelled as group „1" have the absolute brightness $H < 7.8$ and those labelled as group „2" have $H > 7.8$.

only a single DTNO and few SDOs are within Neptune's orbit, but well beyond the orbit of Uranus, in the model.

A large part of this discrepancy can be explained as a consequence of the observational selection effects. A relatively low number of TPs in the model reveals only the most frequent dynamical paths. In the observational sample, there is a large number of small bodies, which can also occur in less frequent paths leading to orbits with a relatively small perihelion distance. Moreover, the dynamics of small, cometary-sized bodies can be influenced by non-gravitational forces, therefore their orbits can earlier evolve to reach the inner planetary region. Since these small bodies can come closer to the Earth, they can acquire an apparent brightness that is high enough for the objects to be discovered from the Earth. In the left plots of Fig. 3 showing the observed distributions, both SDOs and DTNOs are divided into two groups with respect to their absolute magnitude, the value of $H_{lim.} = 7.8$ is chosen to be the limit. We empirically found that just at this $H_{lim.}$-value the distribution of model TPs is mostly consistent with the group of brighter (and, thus, larger) observed objects. Nevertheless, we must state that this explanation of the discrepancy is not fully satisfactory, because there are still a few objects with a relatively high absolute brightness, having small perihelion distances, $q \lessapprox 25$ AU, which are not reproduced in the simulation.

If only the observed objects with $H < 7.8$ are considered, then the spatial structure of DTNOs+SDOs is quite well reproduced by the performed simulation. This can also be documented more exactly. In Fig. 4, we show a gauged-to-unity cumulative semi-major-axis distribution of both observed and simulated DTNO+SDO groups. In the simulated group, the observational bias (see Sect. 2) is imitated considering Trujillo et al.'s (2001) value of the size-distribution index $s = 4.0$. Making the Kolmogorov-Smirnov test, one can find that the hypothesis of a common origin of these distributions can be rejected only with the low probability of 3.5%.

The distribution of inclinations is another proof of the good agreement between the structure of both modelled and observed DTNO+SDO groups. In the case of the observed DTNO+SDO group, we consider only bright ($H < 7.8$) objects, again. The cumulative i-distributions of both groups are shown in Fig. 5. The Kolmogorov-Smirnov test implies the probability of the rejection of common origin of both distributions to be 1.7%. We note that the interval of inclination rises up to $40^o - 45^o$ in both the model and its observed counterpart.

An interesting case is the observed object 127546 (2002 XU93), with $H = 7.9$, belonging to SDOs, in a relatively highly inclined orbit ($i = 78^o$), which is not reproduced within the simulation. Its perihelion distance of 21.0 AU indicates a close approach to Uranus.

The distribution of perihelion distances, q, can be expected to be largely biased by the observational selection. Nevertheless, the upper limit of this element appears to be almost the same, $q \sim 38$ AU, in both observed and modelled samples, as seen in Fig. 3a,b. The only exception is the observed DTNO 145480

(2005 TB190) with $q = 48.3$ AU. We note that no TP occurs in an orbit of the type which is observed in the case of the extraordinary TN object Sedna (MPC-catalogue No. 90377) having $q = 76.3$ AU ($a = 486.8$ AU and $i = 11.9^o$).

The last support of the good agreement of both reality and model is the outer edge of DTNOs which is situated at $\sim$100 AU (see red triangles in Fig. 3). Unfortunately, this agreement can be regarded only as indicative, because the number of DTNOs in the simulation is too small to clearly determine the outer border of the detached TN population. We note that one modelled DTNO orbit is, initially, situated at heliocentric distance of 47.8 AU and other modelled orbits at distances shorter than about 42 AU. Therefore, the situation of the aforementioned border is not influenced by our choice of the outer border of initial PPD at 90 AU.

There are 2 objects, 2000 CR105 and 2004 VN112, with aphelia beyond 100 AU, in observational database, which seem to contradict our conclusion of the 100 AU border. We, however, found that these objects are classified as the resonant objects (according to Gladman et al.'s nomenclature), not as DTNOs. Specifically, 2000 CR105 is in 20:1 MMR and 2004 VN112 in 36:1 MMR with Neptune (the interval of variation of the resonance angle is fairly smaller than 360 degrees).

When we summarize the result concerning the DTNOs+SDOs, it is worth mentioning the ratio of the objects in the OC and these objects. Dones et al. (2004) predicted a much more numerous OC in comparison to DTNOs+SDOs (at that time, they did not distinguish between the DTNOs and SDOs, which were established by Gladman et al. in 2008; they considered these two groups as a single scattered EKB objects). Specifically, they found that the number of cometary nuclei in the OC is an order of magnitude larger than the number of corresponding-sized DTNOs+SDOs. According to our simulation, there are 13 TPs in the outer and 110 TPs in the inner OC, at 2 Gyr. Because of the short outer border, 10^5 AU, up to which we integrated the orbits of TPs in the simulation, the above mentioned population of the outer OC is underestimated by a factor of about 2.5 (Dybczyński et al., 2009). Therefore, the corrected outer-OC simulated population should be about 32.5 TPs and the total OC population in the model at 2 Gyr is about 142.5 TPs. At the same time, the total DTNO+SDO population is represented by 83 TPs, implying that the OC is about 1.7 times more numerous than the DTNO+SDO population. To answer the question about the ratio at present, i.e. about 4.6 Gyr after the zero-time, we compare the exact numbers of TPs in both groups at 1.5 Gyr and 2.0 Gyr. The OC population at 2.0 Gyr was 83% of that at 1.5 Gyr, and the SD+DTN population at 2.0 Gyr was 82% of that at 1.5 Gyr. Due to this small difference and since we did not consider occasional strong stellar perturbations during deep stellar passages through the OC and eventual perturbations by giant molecular clouds, both which have likely increased the erosion rate of the OC population, we can state that our simulation predicts approximately the same ratio of OC and SDO+DTNO populations ($\sim$1.7) in time. Therefore, the relative ratios for the present can roughly be calculated using the model values for 2.0 Gyr and are as given above.

Trujillo et al. (2000) estimated the number of cometary-nucleus-sized objects in the scattered EKB to be about 4×10^9. Neslušan & Jakubík (2005) estimated the population of the outer OC to be 1×10^{11} to 2×10^{11}. The real population of the inner OC is unknown. If we consider the ratio of $\sim$3.4 of inner and outer OC stemming from our simulation, then the real population of the whole OC, based on Neslušan & Jakubík's estimate of the outer-OC population, should be 3×10^{11} to 7×10^{11}. This estimate implies the ratio of OC and DTNO+SDO populations to be 75 to 175. This value is two orders of magnitude larger than the theoretical value predicted with help of our simulation.

However, Neslušan & Jakubík (2005) did not take into account largely different efficiency of the discovery of dynamically new and old comets. This difference yields the reduction of the OC-population of one order of magnitude (Neslušan, 2007), therefore the real OC population is likely to only be 3×10^{10} to 7×10^{10}. So, it is about 7.5 to 17.5 times (one order of magnitude) larger, in fact, than the corresponding-size population of DTNOs+SDOs. It is consistent with the prediction by Dones et al. (2004), but one order of magnitude lower than the prediction by our own simulation. Perhaps, this discrepancy will be clarified in future studies, because the number of OC comets is still not known. Recently, Kaib & Quinn (2010) suggested that the outer OC was enriched by strong gravitational perturbations of the solar birth environment from the inner OC and, thus, the latter may be a dominant source of long-period comets. This unaccounted for comet production lowers the population estimate of the Oort Cloud.

The SDOs and DTNOs are relatively dynamically active groups. Their present-day structure is obviously a result of a recent action (during a period much shorter than the age of the solar system) of outer planets, especially Neptune. In conclusion, it is not therefore surprising that our model of a static planetary configuration can explain the SDO-DTNO dynamical structure quite well.

We also revisited the question of the border between the SDO-DTNO population and the inner OC. This border can exactly be defined as the border between the following dynamical regimes. Bodies in the vicinity of the planetary region are exclusively perturbed by the giant planets, Neptune in particular. In the context of this partial problem, we neglect rare stellar perturbations due to extremely deep passages of stars through the solar system as well as rare mutual perturbations of small bodies at their extremely close approaches. If a planetary perturbation enlarges the aphelion distance of a body, it can become the subject of significant perturbations by the outer perturbers, especially the Galactic tide. So, we can distinguish between the dynamical regimes: (i) a body is perturbed only by planets and (ii) a body is perturbed by both planets and outer perturbers. In the first regime, the bodies at the border are in orbits with

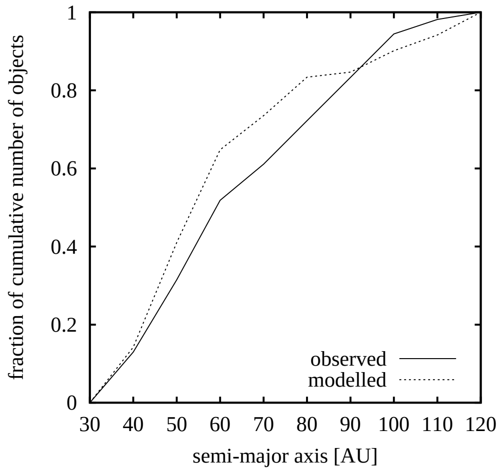

Figure 4. The cumulative semi-major-axis distribution of both modelled and observed bright ($H < 7.8$) SDOs and DTNOs. In the case of the model, the state at 2 Gyr is shown. Both distributions are gauged in such a way that the total number would be equal to unity. In the distribution predicted by our simulation, the primary observational selection effects are imitated, whereby we assume Trujillo et al.'s (2001) value of the index of object-size distribution $s = 4.0$.

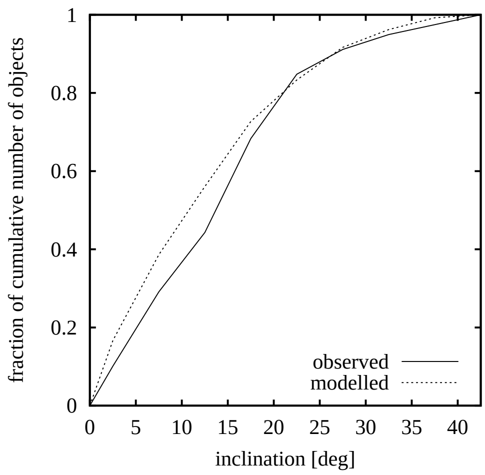

Figure 5. The cumulative distribution of the inclination to the ecliptic of both modelled and observed bright ($H < 7.8$) SDOs and DTNOs. In the case of the model, the state at 2 Gyr is shown. Both distributions are gauged in such a way that the total number would be equal to unity.

the eccentricity approaching unity, while the orbits of those in the second regime have this orbital element in a larger range of values.

Unfortunately, only a small number of TPs in our simulation were in orbits at the border, therefore we can determine the border, in terms of orbital semi-major axis, roughly being in the interval between 1000 and 2500 AU. This agrees with the results of other authors (Duncan et al., 1987; Dones et al. 2004; Emel'yanenko et al., 2007).

5. The classical Edgeworth-Kuiper belt

5.1. The CEKB influenced by Neptune's gravity

In consistency with Gladman et al. (2008), we classify the TNOs in orbits holding the same criteria as DTNOs, but with $e \leq 0.24$, as the objects in the CEKB. In the past, only those objects were regarded as CEKB members that had the semi-major axis between the values corresponding to the 3:2 and 2:1 MMRs. Recently, some CEKB-like objects inside the 3:2 MMR and outside the 2:1 MMR have been discovered. With respect to this fact, Gladman et al. (2008) established a finer non-resonant CEKB classification. The CEKB objects with a between the 3:2 and 2:1 MMRs (i.e. having the semi-major axis $39.4 \leq a \leq 48.4$ AU) constitute the "central" CEKB, those with $a_N < a < 39.4$ AU constitute the "inner" CEKB, and those with 48.4 AU $< a < a_{in}$ the "outer" CEKB.

The distributions of the observed objects as well as the TPs in our simulation at 2 Gyr, which are the members of the CEKB, are shown in Fig. 6 in the $q{-}a$, $e{-}a$, and $i{-}a$ phase spaces. The structure of the modelled CEKB is clearly different from the observed one. The modelled central CEKB occurs only in the vicinity of 3:2, 8:5, 5:3, and 2:1 MMRs, obviously due to the rising eccentricity and inclination of the initial very cold orbits by Neptune. The observed most abundant part of the central CEKB in the 42.5−45 AU interval of semi-major axis is not reproduced in the simulation. The origin of this dense clump of TNOs was only recently explained by Levison et al. (2008). To achieve good agreement with the observed reality, they tuned the initial assumptions of the migration of Neptune.

Except in the vicinity of 3:2 MMR, the prevailing part of orbits of modelled inner CEKB have almost conserved initial very low inclination (Fig. 6f). The eccentricity range of the entire modelled CEKB is smaller than that of the observed CEKB (cf. Fig. 6c,d). It reaches the upper value of about 0.17 (with a single exception of $e \approx 0.2$), while the upper e-value of observed orbits approaches to the definition limit of $e = 0.24$. Similarly, the inclination of modelled-CEKB orbits reaches the upper value of about 20^o (with a single exception of $i \approx 31^o$), while the upper observed value is about 35^o with three objects having the inclination in the $35^o{-}55^o$ interval.

Three orbits of the observed outer-CEKB objects (48639, 2003 UY291, and 2004 XR190), having quite a high eccentricity, are either not reproduced in the

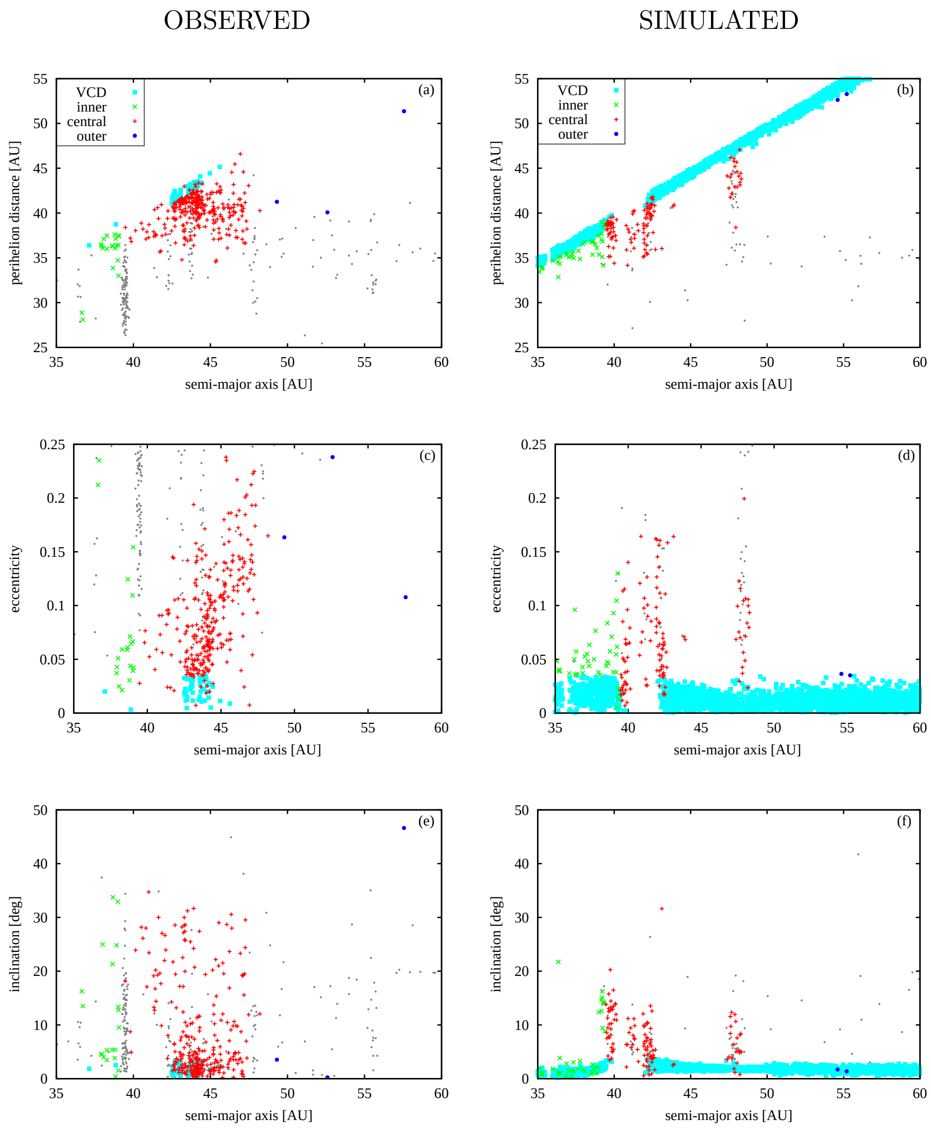

Figure 6. The distribution of the observed objects and simulated TPs, which are classified as the members of the CEKB, in the $q-a$ (plots a, b), $e-a$ (c, d), and $i-a$ (e, f) phase spaces. The left plots (a, c, e) show the observed distributions and right plots (b, d, f) show their modelled counterparts at 2 Gyr. The inner, central, and outer CEKB is distinguished with the help of different symbols, which are black-and-white in the printed and colour in the electronic version of the figure. In addition, the VCD is shown with full squares (sky-blue in the electronic version) and the TN objects/TPs of the other groups with small gray full circles.

simulation, where the eccentricity of a very cold initial population is only slightly risen in the vicinity of 5:2 (2 TPs), 3:1 (10 TPs), and 5:1 (1 TP) MMRs. Eleven TPs at 3:1 and 5:1 MMRs are not seen in Fig. 6, because of the limited a-range.

If we do not consider the initial very cold population (discussed in Sect. 5.2), the central and outer CEKB are practically not reproduced in our simulation. The central CEKB consists only of TPs close (in terms of semi-major axis) to strong MMRs. The inner CEKB is reproduced only qualitatively. Despite this failure of our model, we can recognize one important property of Neptune perturbations of cold, CEKB-type orbits: significant influence of Neptune disappears at the distance of 2:1 MMR. Beyond this distance a few initial cold orbits are slightly excited at the 5:2 MMR and several orbits at the 3:1 MMR. (Such excitations obviously could not replenish the CEKB even in the MMR-neighbouring regions.) The gray points beyond 50 AU in Fig. 6b, f are classified as SDOs and DTNOs and their initial $a < 42.4$ AU (one exception is $a = 47.8$ AU). It seems that a sharp decrease of the number of TPs at the conventional outer border of CEKB at 2:1 MMR can be explained as the outer border at which Neptune's perturbation is effective. This should be valid not only for our model, but for migration models as well, since none of them models has assumed any occurrence of Neptune at a significantly larger distance than its current aphelion.

5.2. The very cold disc

In our simulation, we assumed a very cold initial PPD in the range of heliocentric distance from 4 to 90 AU. It appears that part of this initial population beyond about 33 AU largely survives after 2 Gyr of the dynamical evolution. Only the TPs in 36.3−36.6 AU (corresponding to 4:3 MMR) and 38.9−42.2 AU (3:2, 5:3 MMRs and space between them; this is the region of a strong secular resonance with Neptune (Morbidelli et al., 2008)) intervals beyond 33 AU are moved away at this time. The surviving initial population, which we refer to as the ,,very cold disc" (VCD) hereafter, can be characterized by $e < 0.035$ and $i < 0.065$ rad at 2 Gyr. According to Gladman et al.'s (2008) classification scheme, the VCD belongs to the CEKB. However, we distinguish between the VCD and CEKB of that type, which is well known from observations. In Fig. 6, the TPs of VCD are shown by yellow full circles.

We note that Neptune in its current orbit has been able, during the age of the Solar System of $\sim$4.5 Gyr, to scatter the TN objects up to the heliocentric distance of $\sim$34 AU. The 2-Gyr evolution of the number of objects within 1-AU intervals of heliocentric distance in the range from 31 to 35 AU is shown in Fig. 7. The linear extrapolation of the numbers until 4.5 Gyr implies the survival of a significant number of objects for the distance of $\sim$35 AU. (The number of even more distant objects decreases again due to the 4:3 MMR.)

The survival of the VCD in the simulation indicates that the assumption of a very cold initial PPD extending beyond $\sim$34 AU with the observed CEKB is untenable. Three alternative explanations of this fact can be suggested:

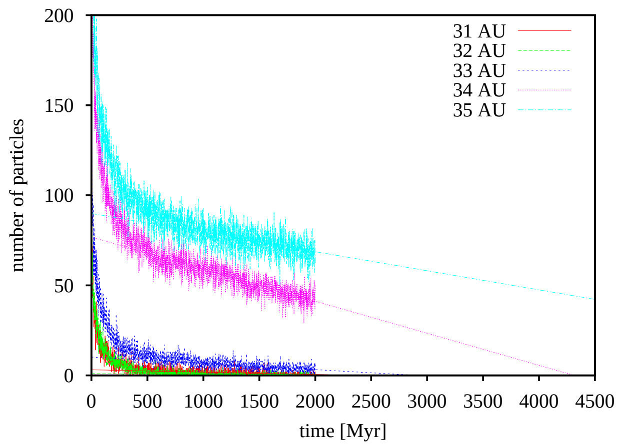

Figure 7. The evolution of the number of TPs in 1-AU wide intervals of heliocentric distance in the range from 31 to 35 AU during the considered period of 2 Gyr. The plots are linearly extrapolated until 4.5 Gyr to predict the surviving numbers of objects, at the given heliocentric distance, at present.

(1) The initial very cold TN population has been destroyed by itself via collisional grinding. This alternative does not seem to be very relevant, however, since the most massive objects should have survived the grinding and should be observed. In addition, the total mass of the initial EKB is estimated to be two to three orders of magnitude higher than the currently estimated mass (e.g. Morbidelli et al., 2008), therefore the net gravity of TNOs must have perturbed orbits of the individual bodies. This implies another alternative explanation that

(2) the TN population was once massive enough to gravitationally erode itself. Within this process, the orbits of TNOs were dynamically excited, i.e. their eccentricities and inclinations significantly rose. This effect should be taken into account in future simulations of the evolution of TN population.

(3) The outer border of the initial PPD was situated at a shorter heliocentric distance than ∼35 AU. Such assumption is also roughly consistent with the Nice model of the late solar-system dynamical evolution (Tsiganis et al., 2005) that the outer border of the outer planetesimal disc was situated at 34 AU. In agreement with the Nice model, the TN population occurred due to the outward migration of Neptune, which pushed some small bodies trapped in the MMRs with this planet into relatively large heliocentric distances.

6. The radial migration of TPs to SDOs and DTNOs

In this section, we answer the question whether some small bodies can migrate from the region of a giant planet into the TN region also in the case when no radial migration and growth of the planets is considered. In the considered initial PPD, the TPs in almost circular orbits with semi-major axis a_o shorter than 8 AU are regarded as those in the Jupiter region. Similarly, the Saturn, Uranus, Neptune, and EKB regions are defined by the TP-semi-major-axis intervals $8 \leq a_o < 15$ AU, $15 \leq a_o < 24$ AU, $24 \leq a_o < 35$ AU, and $a_o \geq 35$ AU, respectively.

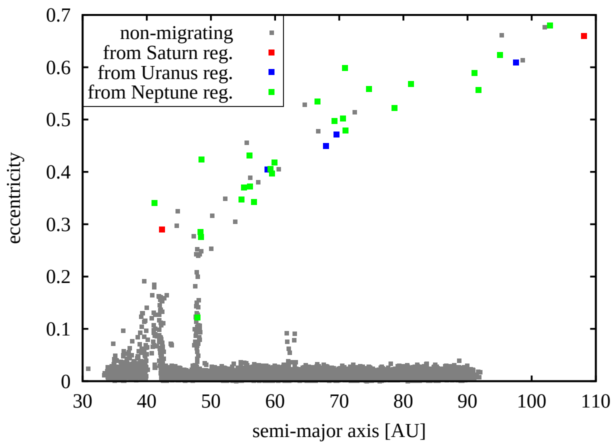

Figure 8. The migration of TPs from the individual planetary regions of the initial PPD into the MMRs, SDOs, and DTNOs. The end-state at 2 Gyr of migrating TPs from the individual regions are distinguished with the help of different symbols, which are black-and-white in the printed and colour in the electronic version of the figure. The TN objects/TPs of the other groups are also shown with small gray full circles.

Actually, the answer on the migration is positive. In Fig. 8, the positions of TPs, which were initially in a region of a planet and ended in the TN region, are shown in $e - a$ space. (Also the migrations from the Neptune region are included if the semi-major axis significantly surpasses the value of 35 AU.)

Specifically, we find 6 TPs in the initial orbits originally assumed in the Neptune region which occur, after 2 Gyr of the dynamical evolution, in the MMRs (2:1, 7:2, 8:1, 14:5, 16:3, and 31:3). A single TP is found to migrate from the Uranus region into MMR 10:1.

The most numerous are the migrations into the SD: 2 TPs migrated there from the Jupiter region, 2 TPs from the Saturn region, 8 TPs from the Uranus region, and 26 TPs from the Neptune region. Into the DTNO-group, a single TP migrated from the Saturn, 5 TPs from the Uranus, and 12 TPs from the Neptune region. Because of the limited a-range of Fig. 8, some of the migrating TPs are not shown.

Our simulation shows that migrations of small bodies from the planetary region into the CEKB is impossible. No single TP migrating in this way appeared. Within the Nice model, Levison et al. (2008) showed that some objects from a distance shorter than 35 AU can still occur in the EKB. However, they also found a deficit of nearly-circular objects in the CEKB. In addition, our conclusion has recently been supported by Parker & Kavelaars (2010) who demonstrated that a binary-bearing component of the cold EKB was emplaced through a gentler mechanism than the Nice model assumes, or was formed in situ.

7. Conclusions

Although the performed simulation of the formation of TN reservoirs, the Oort cloud including, qualitatively predicts almost all observed structural features in the TN region, it proves, at the same time, that the assumption of a dynamically very cold initial PPD ($e \sim 0.01$ and $i \sim 0.01$ rad), which extends beyond the heliocentric distance of about 34 AU, is quantitatively inconsistent with the observed structure of the TN population of small bodies. In future studies, dynamically ,,warmer" initial orbits of small bodies should be assumed.

The following specific discrepancies can be stated:

(1) The part of the initial, dynamically very cold population beyond about 33 AU largely survives after 2 Gyr (with the exceptions of the TPs in 36.3−36.6 AU and 38.9−42.2 AU intervals, where the TPs are moved away).

(2) The relative abundances of the observed and modelled MMRs are different, the difference cannot be explained with the observational selection effects. The ratio of TPs in two prominent MMRs, Plutinos and 2:1 MMR, in the model is considerably smaller than the corresponding observed ratio.

(3) The observed most abundant part of the central CEKB in the 42.5−45 AU interval of semi-major axis is not reproduced in the simulation.

(4) The eccentricities and inclinations of the modelled CEKB orbits are typically smaller than those of the observed CEKB orbits.

(5) The existence of an object in the Sedna-like orbit cannot be explained, because no object appeared in such type of orbit in our simulation.

Two features of the TN population are successfully reproduced in our simulation:

(a) The outer border of the effective Neptune's perturbation coincides with a sharp decrease of the number density of CEKB bodies at the outer border of 2:1 MMR (which has been approximated by the heliocentric distance of 50 AU). Only few orbits near the regions of especially 5:2 and 3:1 MMRs, situated beyond the 2:1 MMR, appear to be slightly changed after 2 Gyr. This coincidence seems to be an explanation of the observed outer border of CEKB if we assume that the CEKB was initially empty and objects currently residing in this region formed in a region closer to the Sun, whereby they were transported, later, into the CEKB by Neptune.

(b) The outer border of the DTNOs (chosen by Gladman et al.'s (2008) classification) is approximately at the same heliocentric distance of 100 AU in both model and observational samples.

Although the SDO and DTNO populations formed at the beginning of the Solar-System existence (during and right after the chaotic phase of the Nice model), their dynamical evolution was found to be relatively fast. Therefore, their current structure is relatively young, formed mostly by Neptune's gravity in the period when this planet has its current mass and orbited the Sun in its current orbit. This conclusion is also proved in our simulation. The other parts of the TN population are dynamically old, with the structure most likely conserved from the beginning of the Solar-System existence, when the planets still grew and migrated to their current orbits. This can be deduced from the fact that the structural features of these parts have been explained much better within the concepts including the planet migration than within our concept of the non-migrating planetary orbits.

Acknowledgements

G.L. thanks PI2S2 Project managed by the Consorzio COMETA, `http://www.pi2s2.it` and `http://www.consorzio-cometa.it` for the computational resources and technical support. L.N. and M.J. thank the project "Enabling Grids for E-sciencE II" (`http://www.eu-egee.org/`) for the provided computational capacity and support in a development of the computer code, which was necessary for a management of tasks on the GRID. They also acknowledge the partial support of this work by VEGA − the Slovak Grant Agency for Science (grant No. 0011).

References

Bowell E., Hapke B., Domingue D., Lumme K., Peltoniemi J., Harris A.: 1989, in *Asteroids II*, eds.: R. Binzel , T. Gehrels and M. Matthews, Univ. Arizona Press, Tucson, 524

Brasser R., Duncan M.J., Levison H.F.: 2007, *Icarus* **191**, 413

Davis D.R., Farinella P.: 1997, *Icarus* **125**, 50

Dohnanyi J.S.: 1968, in *Physics and Dynamics of Meteors, IAU Symp. No. 33*, eds.: Ľ. Kresák and P.E. Millman, Reidel, Dordrecht, 486

Dones L., Weissman P.R., Levison H.F., Duncan M.J.: 2004, in *Comets II*, eds.: M.C. Festou , H.U. Keller and H.A. Weaver, Univ. Arizona Press, Tucson, 153

Duncan M., Quinn T., Tremaine S.: 1987, *Astron. J.* **94**, 1330

Dybczyński P. A., Leto G., Jakubík M., Paulech T., Neslušan L.: 2008, *Astron. Astrophys.* **487**, 345

Dybczyński P. A., Leto G., Jakubík M., Paulech T., Neslušan L.: 2009, *Astron. Astrophys.* **497**, 847
Emeľyanenko V.V., Asher D.J., Bailey M.E.: 2007, *Mon. Not. R. Astron. Soc.* **381**, 779
Gladman B., Marsden B. G., VanLaerhoven C.: 2008, in *The Solar System Beyond Neptune*, eds.: M.A. Barucci , H. Boehnhardt , D.P. Cruikshank and A. Morbidelli, Univ. Arizona Press, Tucson, 43
Holman M.J., Wisdom J.: 1993, *Astron. J.* **105**, 1987
Kaib N.A., Quinn T.: 2010, *Bull. American Astron. Soc.* **41**, 434
Kusaka T., Nakano T., Hayashi C.: 1970, *Prog. Theor. Phys.* **44**, 1580
Leto G., Jakubík M., Paulech T., Neslušan L., Dybczyński P.A.: 2008, *Mon. Not. R. Astron. Soc.* **391**, 1350
Levison H.F., Duncan M.J.: 1993, *Astrophys. J.* **406**, L35
Levison H.F., Morbidelli A., Vanlaerhoven, C., Gomes R., Tsiganis K.: 2008, *Icarus* **196**, 258
Levison H.F., Stern S.A.: 2001, *Astron. J.* **121**, 1730
Malhotra R.: 1993, *Nature* **365**, 819
Morbidelli A., Crida A.: 2007, *Icarus* **191**, 158
Morbidelli A., Levison H., Gomes R.: 2008, in *The Solar System Beyond Neptune*, eds.: M.A. Barucci , H. Boehnhardt , D.P. Cruikshank and A. Morbidelli, Univ. Arizona Press, Tucson, 275
Parker A.H., Kavelaars J.J.: 2010, *Astrophys. J., Lett.* **in press**,
Trujillo C.A., Jewitt D.C., Luu J.X.: 2000, *Astrophys. J.* **529**, L103
Trujillo C.A., Jewitt D.C., Luu J.X.: 2001, *Astrophys. J.* **122**, 457
Tsiganis K., Gomes R., Morbidelli A., Levison H.F.: 2005, *Nature* **435**, 459
Weidenschilling S.J.: 1977, *Mon. Not. R. Astron. Soc.* **180**, 57